ARTICLES

Elastic and mechanical properties of ion-implanted silicon determined by surface-acoustic-wave spectrometry

M. Szabadi and P. Hess
University of Heidelberg, Institute of Physical Chemistry, Im Neuenheimer Feld 253, D-69120 Heidelberg, Federal Republic of Germany

A. J. Kellock, H. Coufal, and J. E. E. Baglin
IBM Almaden Research Center, 650 Harry Road, San Jose, California 95120-6099
(Received 5 January 1998)

Amorphization of silicon by ion implantation at liquid nitrogen temperature was studied by broadband surface-acoustic-wave spectrometry (SAWS) and channelled Rutherford backscattering spectrometry (c-RBS) and the results were compared to simulations computed using TRIM. If the topmost layer of the wafer is completely amorphized, its thickness can be determined by all three methods. In addition, SAWS can measure the density and elastic constants (Young's modulus and Poisson's ratio) of the amorphous layer. Measurements of layer thickness obtained by SAWS and by c-RBS agreed within a few percent in all cases where the fully amorphized silicon layer extended to the silicon surface, as indicated by c-RBS spectra. Damage simulation profiles computed with TRIM also agreed closely with the measured thickness values, using an effective amorphization damage threshold of 5×10^{23} eV/cm^3. The mechanical constants obtained for the amorphized layer were density=(2.30±0.01) g/cm^3; Poisson's ratio=0.27±0.01; Young's modulus=(125±1) GPa. [S0163-1829(98)01638-5]

I. INTRODUCTION

Crystalline silicon (c-Si) has been thoroughly investigated in the last few decades by semiconductor and electronics industries. Due to the use of this element as a source material of both conventional and highly integrated circuits, a large interest in its surface and interface properties exists.[1] In recent years research has partly shifted to an examination of amorphous silicon (a-Si), which can be prepared by many techniques such as vacuum evaporation, sputtering, glow discharge decomposition, and ion implantation. The physical properties of the amorphous layer depend on the preparation conditions.

The interest in amorphous Si lies in two main areas.[2] First, a-Si may be used as a model system of a covalently bonded continuous random network. The differences between a-Si and c-Si illustrate the influence of disorder on the physics of solids. Second, in its hydrogenated form (a-Si:H) it shows semiconducting behavior. The mechanical and elastic properties of this species were already discussed in a previous paper.[3]

Campisano *et al.*[4] examined the mechanisms of amorphization in ion-implanted crystalline silicon. Ion implantation of c-Si produces extensive damage of the crystalline lattice. It has been shown that ion energy, ion mass, substrate temperature, ion dose, and ion flux are the critical parameters governing the amorphization process. Amorphous silicon is a metastable phase of Si with about 15 kJ/mol higher free energy than its crystalline counterpart.[2] The properties of a-Si are well known, yet the mechanisms of its formation by ion bombardment are still under debate.[5] After ion implantation the atomic structure of the damaged layer is generally characterized by the presence of a large number of different defects, both simple and complex.[6] A preexisting planar c-a interface subjected to ion irradiation can move either towards the amorphous side or towards the crystalline side depending on the implantation parameters.[7]

The formation of defects by energetic ion implantation depends on two different stopping processes.[8] High-energy ions lose energy slowly to the electrons in the bombarded lattice. This "electronic stopping" causes few displacements of the atoms in the near surface region of the target. As the ions slow down and approach the end of their range, they will undergo a few atomic collisions and lose energy quickly before coming to rest. This "nuclear stopping" causes the recoil of the struck Si atom, leaving a vacancy in the lattice, and itself creating further ionization and recoils as it loses energy in the host material. At room temperature or higher, the defects created in Si by such recoil displacements are mobile within the ionization cascade, and they may either agglomerate (at high defect density) and thus nucleate growth of the amorphous region, or in regions of low damage they may self-anneal.[4,5] In these cases, the final amorphous layer will tend to be sharply defined, and its thickness will depend on the thermal history of the sample during and after implantation. However, if the implantation is done at liquid nitrogen (LN_2) temperature, the amorphous layer consists only of localized clusters of damage distributed in a way that corresponds closely to the distribution of displacement damage delivered directly during the implantation.[5] "Complete" amorphization results when such clusters are numerous enough to overlap. The process is asymptotic with ion dose,[4] and the degree of disorder that is functionally effective may differ among various practical applications. For example, the disorder required for total dechannelling of He^+ ions in Rutherford backscattering spectrometry (RBS)

 © 1998 The American Physical Society

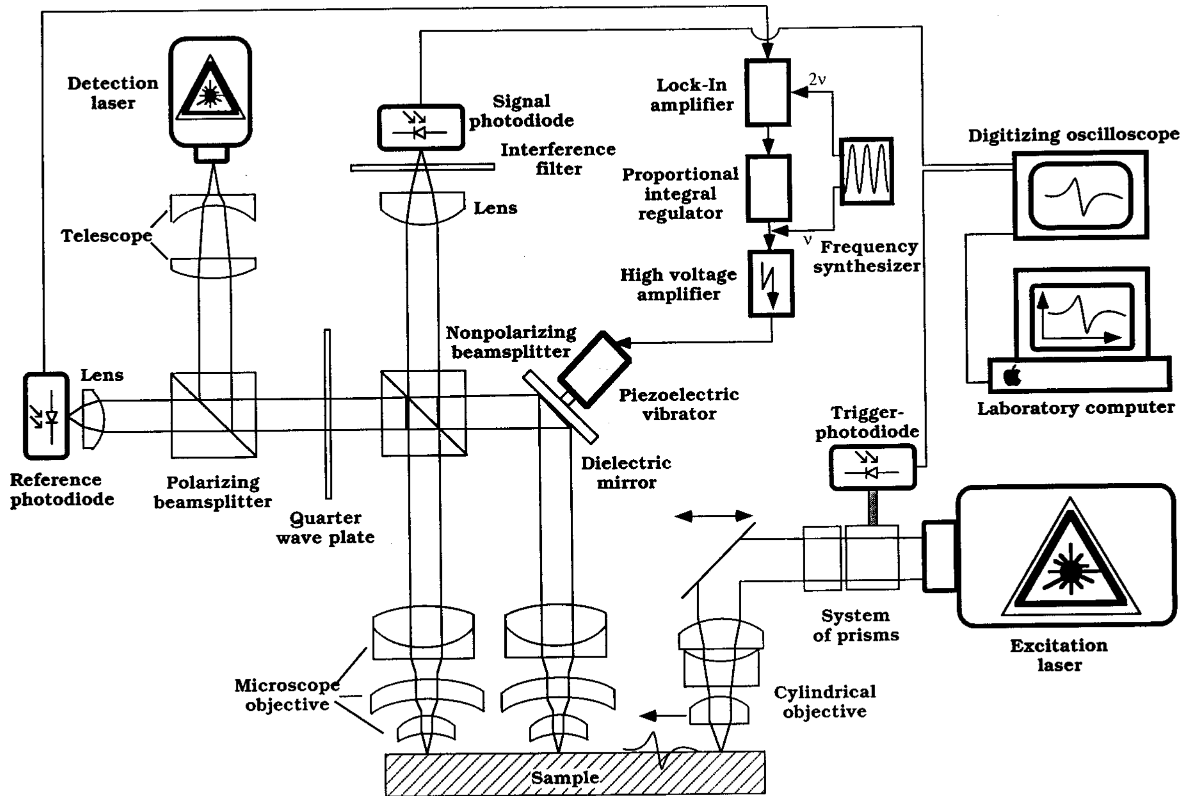

FIG. 1. Experimental setup for surface-acoustic-wave spectrometry.

analysis may not be exactly identical with that which effectively modifies the elastic properties of a damaged silicon layer.

In this experiment, we seek to explore the degree of consistency between (a) characterization of ion-implantation damaged silicon layers with respect to elastic properties and effective thickness, using surface-acoustic-wave spectrometry (SAWS) and (b) measurement of thickness and homogeneity of such amorphized silicon layers using Rutherford backscattering spectrometry in the channeling mode (c-RBS). A further test is applied by estimation of the amorphous layer thickness based on damage profiles calculated with the Monte Carlo program TRIM-95. In order that these profiles should remain approximately proportional to the observed amorphous fraction below saturation, the implantation was carried out at liquid nitrogen temperature.

II. EXPERIMENT

A. SAWS technique

Although the experimental setup of the surface-acoustic-wave spectrometry equipment has been described previously in detail,[9] it is important to provide an up to date overview, since substantial improvements have been made in all parts of the setup. In the experimental arrangement (Fig. 1), a frequency-tripled mode-locked Nd:YAG excitation laser with a wavelength of 355 nm and a pulse duration of 180 ps full width at half maximum (FWHM) was used to excite coherent surface-acoustic-wave pulses. The laser pulses were expanded in one direction by a system of prisms and focused in the second direction onto the sample surface by a system of three cylindrical lenses. The size of the focus line was about 3 μm$\times$12 mm. The pulsed illumination of an absorbing material causes transient expansion of the irradiated volume and ablation of material. This launches nearly planar SAW pulses with a broad frequency spectrum that extends to 700 MHz.

After traveling for a distance of 15 to 35 mm, these pulses were detected at two locations spaced 12 mm apart along the direction of propagation by a modified Michelson interferometer in which the inspected surface served as both of the interferometer mirrors. The beam of a frequency-doubled diode pumped polarized cw-Nd:YAG detection laser was expanded by a telescope and passed through an optical insulator consisting of a polarizing beam splitter and a quarter-wave plate. Then it was divided into sample and reference beams of equal intensities by a nonpolarizing beam splitter. One of these beams was then reflected by a dielectric mirror mounted on a piezoelectric vibrator and focused onto the sample surface to a spot of about 1 μm diameter by a microscope-objective with a numerical aperture of 0.5. The second beam was focused directly onto the surface by an identical objective. The light reflected by the sample was collected by the corresponding microscope objective and, after again passing the nonpolarizing beam splitter, the interference signal was detected by the signal photodiode, which was protected from light of the excitation pulse by a suitable filter. The beam reflected towards the laser was polarized perpendicularly to its initial direction of polarization and was directed out of the interferometer by the polarizing beam splitter. The signal photodiode was a fast, low-noise PIN silicon diode (Hamamatsu S4753) with a bandwidth of 1.5 GHz. The electronic circuitry reduced this value to about 1 GHz. The signal from this photodiode was amplified and

recorded by a fast digital storage oscilloscope, which was triggered by a UV-sensitive photodiode and connected to a laboratory computer.

The interferometer sensitivity is a function of the phase difference between the sample and the reference beams, which are subject to thermal and mechanical noise. Therefore a stabilizing circuit was necessary to lock the interferometer to its most sensitive operating point. This was achieved by a feedback system which automatically compensated for low-frequency deviations from this point, thus assuring the constant sensitivity required for measuring short SAW pulses. In practice, the piezoelectric transducer was oscillated with an amplitude of 15.6 nm at 2 kHz by a sine voltage from a frequency synthesizer in order to modulate the path length of one of the interferometer arms. When the operating point of the interferometer deviated from the optimum position, corresponding to a phase difference of λ/8 between the two interfering beams, a weak component with the doubled modulation frequency arose in the photodiode output signal. This component was detected by a lock-in amplifier. The ''in-phase'' signal was then processed by a proportional-integral regulator to supply a correction voltage for the high voltage amplifier supplying the piezoelectric vibrator. The sensitivity of the arrangement described above was sufficient to resolve a surface displacement of 0.5 nm with 1 GHz bandwidth for a single shot and could be further improved by averaging.

The pulse wave forms were measured as a function of time at two points A and B, which indicate the distances of the two probe spots from the excitation line source. Both transient wave forms were Fourier transformed and then the corresponding amplitude spectra $[A_A(\omega), A_B(\omega)]$ and phase spectra $[\varphi_A(\omega), \varphi_B(\omega)]$ were calculated. The dispersion relation $v(\omega)$, i.e., the phase velocity of the acoustic wave as a function of the angular frequency, could be determined by the method of Ref. 10.

To calculate the elastic and mechanical properties of a fully amorphized surface layer, knowledge of the dispersion relation is sufficient.[1] Apart from the measurement of the experimental dispersion curve it is essential to develop an appropriate theoretical description of the problem.

Solutions for systems consisting of a single layer having different mechanical and elastic properties from those of its substrate were reviewed by Farnell and Adler[11] and adapted for our purposes in the present study. In the case of an isotropic layer (which corresponds to the fully amorphized topmost layer of an ion-implanted wafer), there exist four unknown parameters of the layer: density, thickness, Young's modulus, and Poisson's ratio. The values for all four parameters can be derived by fitting the theoretical dispersion curve to the measured one.

B. Silicon amorphization

For all implantations, the ion beam was electrostatically rastered over the target area, and the dose was measured with sampling Faraday cups at the periphery of that area. The beam dose uniformity across the implant area was checked by RBS and found to be about ±1%. The beam current used was typically 20 μA. The sample carrier was liquid nitrogen cooled during implantation to prevent self-annealing of the samples during implantation. All implantations were performed in a vacuum of at least 3×10^{-7} Torr.

We prepared several sets of ion-implanted silicon samples, which could be classified into four different groups. Each sample (4 cm×4 cm×3 mm) was cut parallel to the {111} plane, and two identical squares 2 cm×2 cm were implanted simultaneously on each wafer. Each group of implantations was designed to test a different set of variables, as detailed below.

(a) Dose dependence: Seven wafers were implanted with 1250 keV Ar^+ ions at doses of 5×10^{13}, 1×10^{14}, 5×10^{14}, 1×10^{15}, 5×10^{15}, 1×10^{16}, and 5×10^{16} ions/cm^2, respectively.

(b) Energy dependence: Five wafers were implanted with 5×10^{15} Ar^+ ions/cm^2 at energies of 250, 500, 750, 1000, and 1250 keV, respectively.

(c) Ion mass dependence: Five wafers were implanted with 5×10^{15} ions/cm^2 at various energies chosen such that the implantation depth was about 1.3 μm for the ion species Ar^+, O^+, He^+, D^+, and H^+.

(d) Dependence on annealing temperature: Three wafers were implanted at LN_2 temperature with Ar^+ ions of different doses and energies (see Table III) and subsequently annealed at temperatures of 180, 330, and 530 °C.

One sample, with a dose of 5×10^{15} Ar^+ ions/cm^2 at an implantation energy of 1250 keV was common to all groups (a)–(c) and was similar to the first sample in group (d).

Channelled RBS was used in this study to determine the extent of amorphization in each sample, and the profile and depth of the amorphized layer. With this method, well collimated 2.3 MeV helium ions are directed into the sample and the energy loss spectrum of the backscattered ions is recorded. The orientation of the sample with respect to the incident ion beam is varied to align the incident beam with the crystalline axis near normal to the wafer, and thus exploit the large difference in channelled RBS yield between crystalline and amorphous Si. A full description of RBS and the channeling technique is beyond the scope of this paper, but is described in full detail in Ref. 12.

In addition to the experimental methods SAWS and RBS, the ion-induced damage distribution was calculated using TRIM (transport of ions in matter), a Monte Carlo type simulation of ion-atom collisions.[13] For c-RBS and TRIM, the depth scale is determined by the He^+ stopping power S in silicon.[12] A degree of uncertainty in the value of S persists, despite decades of measurements. In this work, the S values were derived using the correction factor of 0.92 proposed by Climent-Font,[14] on the values indicated by the tables of Ziegler *et al.*[15] It is believed that this value is also consistent with that used in TRIM-95 simulation routines.

III. RESULTS

A. SAWS measurements

As an example, Fig. 2 shows the ⟨112⟩-dispersion curves of the SAWS study of energy dependence [group (b)]. All wafers were measured in ⟨112⟩ as well as ⟨110⟩ directions (i.e., the surface-acoustic-wave traveled on the {111} surface of the wafer along the ⟨112⟩ and ⟨110⟩ direction, respectively). Hence, for each wafer two dispersion curves were

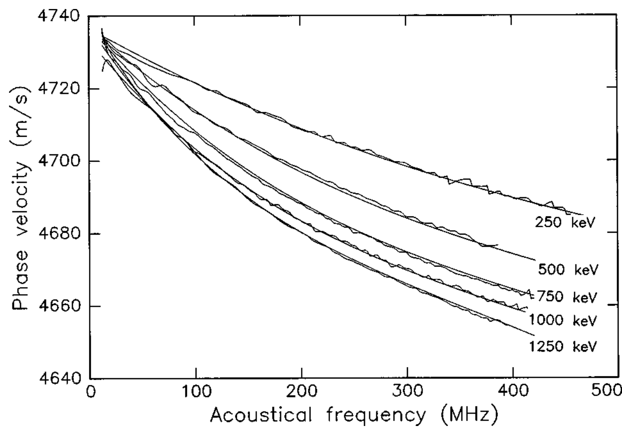

FIG. 2. Experimental dispersion curves measured by SAWS, including simulations, for samples implanted with 5×10^{15} Ar^+ ions/cm^2 at various energies [group (b)].

measured which were simultaneously fitted by the theoretical model. Thus the measurement errors could be approximately halved compared to a fit in only one direction. The negative slope of the dispersion curves indicates that the sound velocities of the implanted region are smaller than the comparable values of the crystalline bulk material and from this it follows that the material is made "softer" by ion implantation.

The SAWS dispersion curves were fitted using the model of Ref. 3, which makes the assumption of a single homogeneous amorphous layer on top of the crystalline substrate. The values for Young's modulus, Poisson's ratio, density and thickness thus deduced for the amorphous layer are displayed in Tables I, II, and III, corresponding to the sample groups identified above as (a), (b), and (d).

In some cases, the SAWS curves were clearly ill behaved, or the signals were small or lost in the background noise. Data from such samples have been shown in parentheses in these tables. As we shall see, in most of these cases, the failure is attributable to incomplete conversion of the silicon to a homogeneous amorphous layer, a situation which would invalidate the algorithm used to interpret SAWS data in any case.

B. Channeling data

Figures 3–5 show the spectra obtained from RBS of 2.3 MeV He^+ ions at 170°, with the samples aligned for optimum channeling. Figure 3 also includes for reference a "random" spectrum obtained with the sample tilted at 7° and rotated continuously to avoid channeling effects, and a channelled spectrum from a nonimplanted sample.

Figure 3 overlays spectra from the sample set (a), displaying dose dependence for implantation of 1250 keV Ar^+. For the lowest two doses, it is evident that most crystalline order has remained, while relatively local damage has occurred near the end of range of the ions. At a dose of 5×10^{14} ions/cm^2, complete dechanneling is seen for most of the ion range, where the spectrum coincides with the "random" spectrum; at greater depths, the RBS yield is again reduced, due to channeling of ions that emerge from the amorphous layer into the undamaged silicon below. At the higher doses, the amorphized layer evidently becomes somewhat thicker. The channeling profiles thus indicate clearly

TABLE I. Experimental data from c-RBS and SAWS, for a-Si layers formed by implantation at LN_2 temperature of 1250 keV Ar^+ ions at a variety of doses. Matching TRIM values for layer thicknesses are also shown. For the first two samples, c-RBS showed incomplete amorphization, hence no thickness values are listed from c-RBS or TRIM; corresponding values from SAWS are also therefore presumed to be invalid, and they are shown in parentheses. The value γ_{max} specifies the product of the largest occurring wavenumber and the layer thickness for SAWS, and is a measure of the information content of the dispersion curve. Experimental uncertainties quoted represent the reproducibility of each point. The additional systematic (scale) uncertainty in thickness value estimated for RBS is ±3%, and for SAWS it is ±1%.

	RBS	TRIM	SAWS				
Dose (ions /cm^2)	Thickness of amorphous layer (μm)	Thickness of amorphous layer (μm)	Thickness of amorphous layer (μm)	Young's modulus (GPa)	Poisson's ratio	Density (kg/m^3)	γ_{max} ⟨110⟩ / γ_{max} ⟨112⟩
5E13			(0.51±0.06)	(151±5)	(0.27±0.03)	(2350±60)	(0.35)
							(0.34)
1E14			(0.92±0.04)	(142±3)	(0.27±0.02)	(2330±50)	(0.51)
							(0.62)
5E14	1.41±0.02	1.41	1.44±0.04	127± 2	0.27±0.01	2310± 30	1.01
							0.78
1E15	1.46±0.02	1.44	1.45±0.05	126± 3	0.25±0.02	2290± 40	0.87
							0.78
5E15	1.49±0.02	1.52	1.48±0.03	126± 3	0.26±0.02	2310± 30	0.91
							0.80
1E16	1.52±0.02	1.53	1.52±0.04	123± 4	0.26±0.02	2290± 40	0.87
							0.82
5E16		1.58	1.55±0.05	129± 3	0.27±0.02	2320± 40	0.78
							0.73

TABLE II. Experimental data from c-RBS and SAWS, for a-Si layers formed by implantation of 5×10^{15} Ar^+ ions at several different energies. Matching TRIM values for layer thickness are also listed.

	RBS	TRIM	SAWS				
Implant energy (MeV)	Thickness of amorphous layer (μm)	Thickness of amorphous layer (μm)	Thickness of amorphous layer (μm)	Young's modulus (GPa)	Poisson's ratio	Density (kg/m^3)	γ_{max} ⟨110⟩ / γ_{max} ⟨112⟩
0.25	0.47±0.02	0.46	0.50±0.02	121±3	0.28±0.02	2300±30	0.32 / 0.30
0.50	0.78±0.02	0.80	0.83±0.01	123±3	0.28±0.01	2300±30	0.72 / 0.60
0.75	1.04±0.02	1.10	1.12±0.02	125±3	0.27±0.02	2300±30	0.63 / 0.65
1.00	1.22±0.02	1.33	1.35±0.02	126±2	0.26±0.02	2310±30	0.57 / 0.66
1.25	1.49±0.02	1.52	1.48±0.03	126±3	0.26±0.02	2310±30	0.91 / 0.80

that for 1250 keV Ar^+, doses of 5×10^{14} ions/cm^2 and higher will produce a homogeneously amorphized layer extending from the sample surface, while for smaller doses, the damaged layer will be nonuniform, and amorphization near the surface is incomplete. Consequently, such smaller doses can not have produced samples that satisfy the homogeneity criterion for a single amorphous layer that SAWS requires. Thus for 1250 keV Ar^+, only those SAWS results from doses greater than 5×10^{14}/cm^2 can be fully valid.

For each case, the thickness of the amorphized layer was determined, using RUMP (Ref. 16) to simulate that layer, and including the effects of energy resolution and straggling. In order to express these thicknesses in micrometers, RUMP assumed a density of 2.32 g/cm^3, and He^+ ion stopping power values reduced by 8% as proposed by Ref. 14. The depth values obtained for the amorphous layer are displayed in Table I for comparison with the SAWS results.

Figure 4 displays the channeling spectra corresponding to set (b), Ar^+ implantation at several energies at a fixed dose of 5×10^{15} ions/cm^2. As expected, the depths of amorphization are smaller for lower energies. In all cases, a completely amorphized layer is indicated, and the corresponding layer thicknesses are compared with SAWS data in Table II.

Figure 5 shows the channeling spectra from set (c), implantations of a variety of ion species at a fixed dose with similar ranges. Unfortunately, only the Ar^+ implanted sample developed a fully amorphized, homogeneous single layer at the chosen dose. The other ions succeeded only in producing varying amounts of local damage in a buried layer, with an ordered Si layer surviving on top. The sharpness of the amorphous layer for the O^+ implants, compared with that of the partially amorphized layers of Fig. 3, suggests that the samples may have had inadequate cooling during oxygen bombardment. Clearly, the basis of the SAWS model was not fulfilled for any of these samples except the Ar^+ implant. Thus, it is no surprise that the SAWS dispersion effect proved to be very low for these samples (of the order of the noise), and no elastic properties could be deduced. It is perhaps interesting to note that the SAWS failed so completely even in the samples where a well defined amorphous layer existed beneath an undamaged layer of silicon.

C. TRIM modeling

TRIM Monte Carlo simulations can be used to calculate for each incident ion, as a function of depth, the density of en-

TABLE III. Effects of annealing on the parameters of an a-Si layer, as measured by SAWS. Results are shown for three differently Ar^+-implanted samples.

Implant energy (MeV)	Dose (ions/cm^2)	Procedure	Thickness of amorphous layer (μm)	Young's modulus (GPa)	Poisson's ratio	Density (kg/m^3)	γ_{max}
1.20	1E16	as implanted	1.60±0.15	122±6	0.23±0.04	2260±70	0.87
		180 and 330 °C	1.65±0.12	131±4	0.22±0.03	2270±50	0.80
		530 °C	1.65±0.15	140±7	0.21±0.03	2300±50	1.38
0.25	1E16	as implanted	0.50±0.03	121±5	0.24±0.04	2280±50	0.33
		180 and 330 °C	0.50±0.04	135±7	0.25±0.03	2330±70	0.34
		530 °C	0.48±0.05	142±7	0.23±0.03	2350±70	0.47
0.25, 0.5,	4E16	as implanted	1.40±0.10	121±6	0.24±0.03	2260±50	0.79
0.8, 1.2		180 and 330 °C	1.42±0.08	130±5	0.22±0.04	2290±40	0.78
		530 °C	1.47±0.10	132±6	0.22±0.03	2290±40	0.89

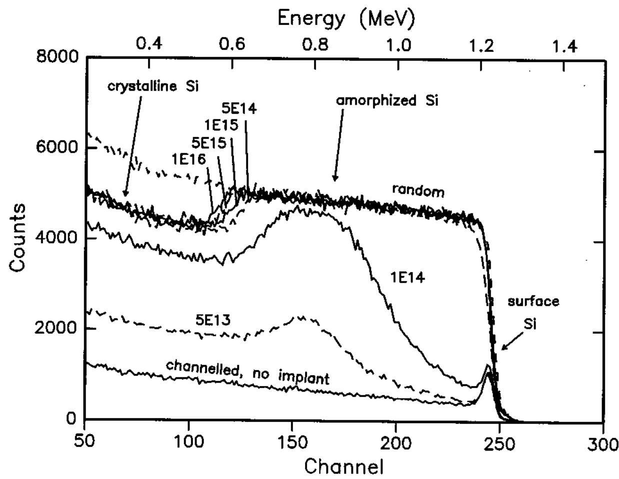

FIG. 3. Channeling RBS spectra from samples of group (a), displaying dose dependence for amorphization due to 1250 keV Ar^+ implantation. (See Table I.)

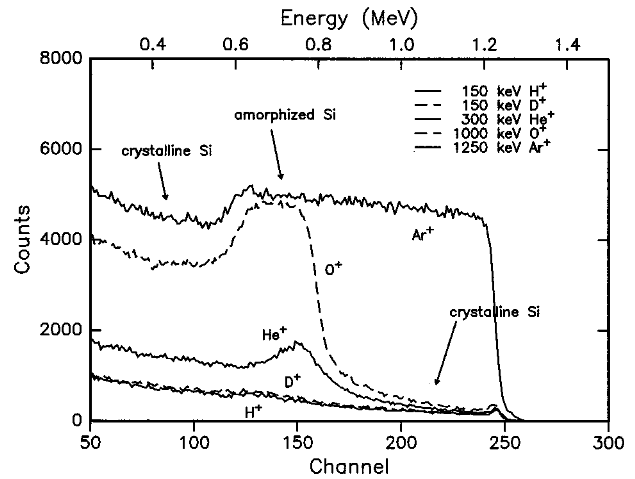

FIG. 5. Channeling RBS spectra from samples of group (c), showing the effects of various ion species and implantation energies at a dose of 5×10^{15} ions/cm^2. Only the Ar^+ provided the homogeneous amorphized layer required for SAWS.

ergy deposition via all recoil collisions, both primary and secondary, that produce vacancies in the silicon. We may refer to this quantity as the recoil energy density E_R, expressed in units of (eV per Å) per incident ion. By multiplying E_R by the dose D of implanted ions (ions per cm^2), we obtain a calculated value for the total energy density invested in damage creation during a particular implantation run, which we call $E_d = E_R \times D$, and which is expressed in (eV per cm^3).

It will be our simple premise for the following discussion that E_d at a given depth d should scale with the degree of disorder produced in silicon, up to some particular ''threshold'' value of E_d at which amorphization is essentially complete, as indicated experimentally by total loss of channeling in RBS (i.e., the spectrum matches the ''random'' spectrum). The depth of the totally amorphized layer may then be measured by the length of the intercept of the threshold line with the E_d depth distribution curve.

Figure 6 shows TRIM-based E_d curves corresponding to 1250 keV Ar^+ implantation at the doses used in this experiment. Starting with the criterion of full amorphization for the 5×10^{14} ion/cm^2 dose, but no saturation for 1×10^{14} ion/cm^2, and using the RBS depths of Table I as indicators, it is found that a single ''threshold'' level of 5.0×10^{23} eV/cm^3 provides remarkably good consistency with the RBS data, as shown in the TRIM column of Table I. This arbitrary threshold level is drawn in Fig. 6, and the tabulated depths represent intercepts for which the ''damage'' curve exceeds that threshold level.

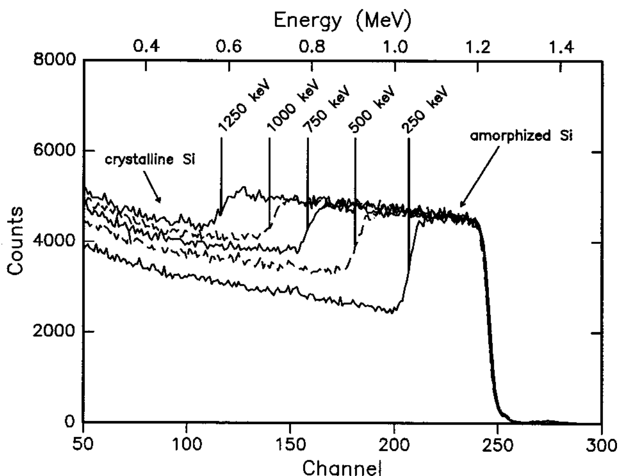

FIG. 4. Channeling RBS spectra from samples of group (b), showing dependence on Ar^+ ion energy for implantation at a dose of 5×10^{15} ions/cm^2. (See Table II.)

It is interesting to note that, as one might expect, the same threshold level may be applied to the data set for various Ar^+ ion energies [set (b)], with apparent consistency with RBS. The TRIM distributions for this fit are shown in Fig. 7, and the depths listed in Table II.

IV. DISCUSSION

A. Amorphous layer thickness

In all cases where c-RBS indicates a single homogeneous amorphous silicon layer extending to the surface, there is

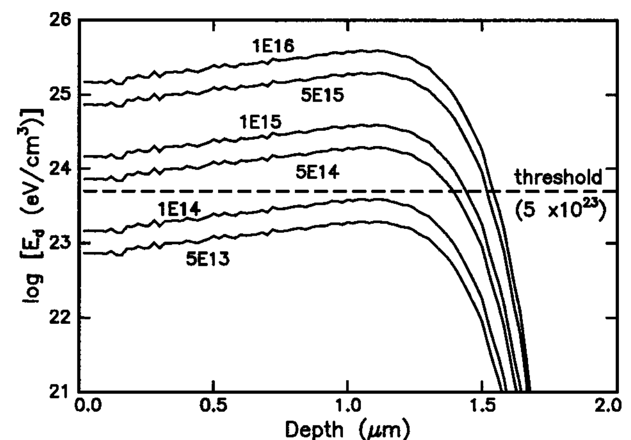

FIG. 6. TRIM simulations of damage density as a function of depth for 1.25 MeV Ar^+ in Si. To simulate various doses shown, the TRIM output was scaled accordingly. Good agreement with c-RBS profile thicknesses is obtained by assuming the ''threshold'' density shown as that which effectively causes complete amorphization for the purposes of c-RBS. (See Table I.)

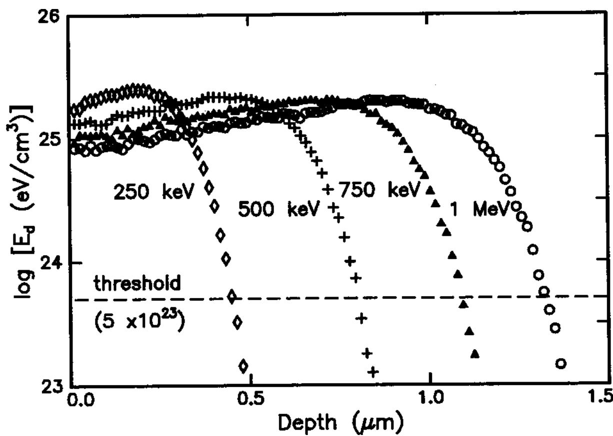

FIG. 7. TRIM simulations, similar to those of Fig. 6, for implantation of 5×10^{15} Ar^+/cm^2 at several different energies. The same amorphization ''threshold'' is used to obtain a-Si thickness values shown in Table II.

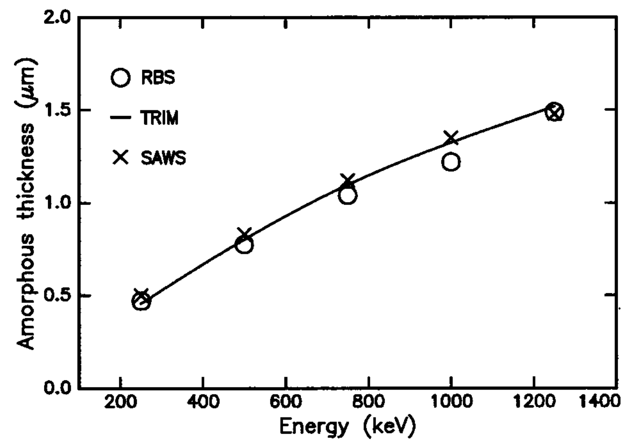

FIG. 9. Comparison of the effective thickness of amorphous layers as derived from c-RBS, SAWS, and TRIM, for 5×10^{15} Ar^+ implants at several energies.

excellent agreement between thickness values derived from c-RBS and from SAWS. TRIM simulations also agree excellently if the assumption is made that a single ''threshold'' level of directly created damage determines the effectively complete amorphization of silicon wherever that threshold has been exceeded.

The agreement between amorphous thickness values obtained by TRIM, c-RBS, and SAWS is documented in Tables I and II and displayed clearly in Figs. 8 and 9. From this agreement, we conclude that the amorphous state damage criterion is essentially identical for c-RBS and for SAWS. Also, it appears from the agreement of TRIM that amorphization results from an E_d value of approximately 5×10^{23} eV/cm^3 produced by all displacement processes during implantation of Ar^+ at liquid nitrogen temperature.

A clear correlation is evident between cases where c-RBS has identified either inhomogeneous or unsaturated amorphization, and cases where SAWS either fails to respond or its interpretation with a bilayer algorithm leads to strange results. For valid SAWS measurements, the amorphous layer must be complete. TRIM evidently provides a valid tool for predicting the dose and energy of a different implantation species that would be required in order to create a functional SAWS sample.

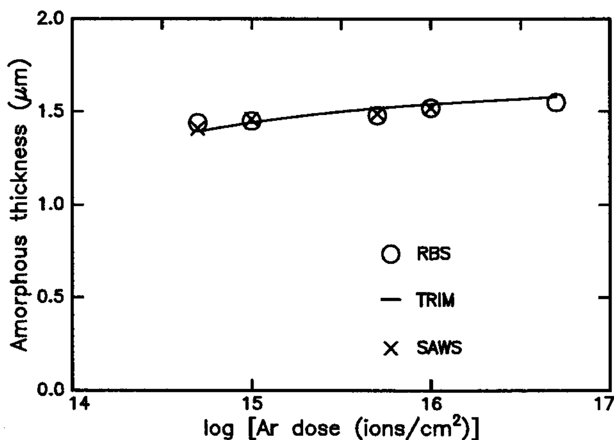

FIG. 8. Comparison of the effective thickness of amorphous silicon layers, as derived from c-RBS, SAWS, and TRIM, for 1250 keV Ar^+ implants at various doses. Error bars represent the degree of reproducibility of each measurement. Systematic (scale) uncertainties may also apply: ±3% for RBS; ±1% for SAWS.

B. Elastic properties of amorphous silicon

Density. For the entire set of fully amorphized Ar^+ implanted samples (Tables I and II), all the values obtained from SAWS are consistent within their estimates of uncertainty. The mean value for the ensemble is (2.30 ± 0.01) g/cm^3. This may be compared with the value of 2.33 g/cm^3 attributed to crystalline Si, indicating only a 1.3% difference in this case. This is consistent with the observation of Custer *et al.*,[17] in which the density of self-ion implanted Si was observed to be 1.8% less than that of crystalline Si. Table III refers to a set of samples amorphized with different Ar^+ implantation conditions. The mean a-Si density indicated by SAWS for them is (2.27 ± 0.04) g/cm^3, a value that rose to (2.31 ± 0.05) g/cm^3 after the samples were annealed at 530 °C for 3 h. The physical significance, if any, of these changes is not clear, although some degree of recrystallization would not be unexpected.

Poisson's ratio. The values of Poisson's ratio for the data sets of Tables I and II are remarkably constant, within the estimates of uncertainty. Their mean value is (0.27 ± 0.01). Again, the value differs from that obtained from the samples of Table III, namely, (0.24 ± 0.02) before annealing and (0.22 ± 0.02) after annealing.

Young's modulus. Again, for the data of Tables I and II, using only the fully amorphized samples, a consistent value of Young's modulus appears. The mean value is (125 ± 1) GPa, which may be compared with a value of 160 GPa for crystalline silicon. The annealing results of Table III show a systematic increase in Young's modulus with annealing temperature, rising to about (135 ± 5) GPa. This relatively small effect indicates that the silicon lattice has not completely lost its identity. It may be surmised that the reason for this is that every silicon atom that is removed from its lattice site, leaving a location of very high free energy, will be attracted by a similar region several Å away which reduces the stress and/or strain of the lattice at this point. By

means of the constraint-counting model[18,3] it was possible to calculate the mean network coordination number (MNC), which indicates the number of bonds that every silicon atom develops on the average. For an assumed mean crystalline value of Young's modulus of 160 GPa, we calculate MNC $=3.75$ for amorphous silicon with 120 GPa. Theoretically a minimum MNC of 2.4 can be reached for a Young's modulus of zero at the point where the network disintegrates. For the reasons mentioned above, this situation is evidently far from being attained by ion implantation.

IV. CONCLUSION

We have demonstrated the applicability of surface-acoustic-wave spectrometry for simultaneous determination of mechanical and elastic properties (thickness, density, Poisson's ratio, and Young's modulus) in silicon layers amorphized by ion implantation. RBS channeling profiles provided essential confirmation of the complete layer amorphization necessary for direct interpretation of SAWS in this way, and independently confirmed the layer thicknesses derived from SAWS. Separate confirmation was provided by TRIM damage simulations, which displayed agreement with observed layer thicknesses consistent with a model in which functionally complete amorphization is reached wherever the calculated damage-creating energy density E_d exceeds an empirically determined threshold of 5×10^{23} eV/cm^3. It is expected that the TRIM model applies only when implantation is done at or below LN_2 temperature, where vacancy mobility is low.

ACKNOWLEDGMENTS

Financial support of this work from the Bundesministerium für Bildung, Wissenschaft, Forschung und Technologie (BMBF) under Contract No. 13N6005 is gratefully acknowledged. One of the authors (M.S.) is thankful to BMBF for enabling a stay at IBM-ARC to plan and commence the experiments. The authors also wish to thank V. E. Gusev for helpful discussions, and T. T. Bardin for helpful collaboration in evaluation of TRIM data, and for many helpful discussions.

[1] W. Mönch, *Semiconductor Surfaces and Interfaces* (Springer-Verlag, Berlin, 1995).

[2] S. Roorda, W. C. Sinke, J. M. Poate, D. C. Jacobson, S. Dierker, B. S. Dennis, D. J. Eaglesham, F. Spaepen, and P. Fuoss, Phys. Rev. B **44**, 3702 (1991).

[3] R. Kuschnereit, H. Fath, A. Kolomenskii, M. Szabadi, and P. Hess, Appl. Phys. A: Solids Surf. **A61**, 269 (1995).

[4] S. U. Campisano, S. Coffa, V. Raineri, F. Priolo, and E. Rimini, Nucl. Instrum. Methods Phys. Res. B **80/81**, 514 (1993).

[5] M. K. El-Ghor, O. W. Holland, C. W. White, and S. J. Pennycook, J. Mater. Res. **5**, 352 (1990).

[6] A. V. Buravlyov, A. F. Vyatkin, V. K. Egerov, V. V. Kireiko, and A. P. Zuev, Nucl. Instrum. Methods Phys. Res. B **55**, 642 (1991).

[7] T. Lohner, E. Kótai, N. Q. Khan, Z. Tóth, M. Fried, K. Vedam, N. V. Nguyen, L. J. Hanekamp, and A. van Silfhout, Nucl. Instrum. Methods Phys. Res. B **85**, 335 (1994).

[8] H. Sayama, A. Kinomura, Y. Yuba, and M. Takai, Nucl. Instrum. Methods Phys. Res. B **80/81**, 587 (1993).

[9] A. Neubrand and P. Hess, J. Appl. Phys. **71**, 227 (1992).

[10] A. Neubrand and P. Hess, Mater. Sci. Eng., A **122**, 33 (1989).

[11] G. W. Farnell and E. L. Alder, in *Physical Acoustics*, edited by W. P. Mason and R. N. Thurston (Academic, New York, 1972), Vol. IX, pp. 35 ff.

[12] W.-K. Chu, J. W. Mayer, and M-A. Nicolet, *Backscattering Spectrometry* (Academic, New York, 1978).

[13] J. P. Biersack and L. Haggmark, Nucl. Instrum. Methods Phys. Res. **174**, 257 (1980) (TRIM program for PCs available from J. F. Ziegler, IBM-Research, 28-0, Yorktown Heights, NY 10598).

[14] J. M. Gilperez, A. Climent, J. M. Martinez-Duart, and J. Perriere, in *EPM'89*, edited by K. Hohmuth and E. Richter, Physical Research (Akademie-Verlag, Berlin, 1990), Vol. 13, p. 268; A. Climent-Font, U. Watjen, and H. Bax, Nucl. Instrum. Methods Phys. Res. B **71**, 81 (1992).

[15] J. F. Ziegler, J. P. Biersack, and U. Littmark, *The Stopping and Range of Ions in Solids* (Pergamon, New York, 1985).

[16] RUMP program, L. R. Doolittle, Nucl. Instrum. Methods Phys. Res. B **9**, 344 (1985). (Available from Computer Graphic Services, Lansing, NY.)

[17] J. S. Custer, M. O. Thompson, D. C. Jacobson, J. M. Poate, S. Roorda, W. C. Sinke, and F. Spaepen, Appl. Phys. Lett. **64**, 437 (1994).

[18] J. Robertson, Phys. Rev. Lett. **68**, 220 (1992).